Applied Catalysis B: Environmental 187 (2016) 399–407

Contents lists available at ScienceDirect

Applied Catalysis B: Environmental

journal homepage: www.elsevier.com/locate/apcatb

# Identification of Cu surface active sites for a complete nitrate-to-nitrite conversion with nanostructured catalysts

C. Roy, J. Deschamps, M.H. Martin, E. Bertin, D. Reyter, S. Garbarino, L. Roué, D. Guay*

*INRS—Énergie, Matériaux Télécommunications, 1650 Lionel-Boulet Blvd., P.O. Box 1020, Varennes, Quebec J3X 1S2, Canada*

ARTICLE INFO

*Article history:*
Received 15 November 2015
Received in revised form 12 January 2016
Accepted 17 January 2016
Available online 21 January 2016

*Keywords:*
Electrodeposition
(100) Pt surfaces
Underpotential deposition
Cu monolayer
Cu sub-monolayer
Selective stripping
Nitrate reduction

ABSTRACT

Nitrate reduction on Pt nanostructured films, $Pt_{NSF}$, with an extended surface area (roughness factor of ca. 30), and close to 50% of (100) surface sites modified by Cu adatoms through underpotential deposition ($Cu_{upd}/Pt_{NSF}$), has been studied by means of linear sweep voltammetry (LSV), electrolysis at constant potential, and chemical analysis of the formed products. According to the LSV curves, the adsorption and reduction of nitrates occur preferentially at Cu(100) surface sites and at a potential positive (+0.15 V) of the hydrogen reversible potential. In these conditions, the nitrate-to-nitrite conversion is achieved on the Cu(100) sites, with a faradic efficiency in excess of 95%, and a conversion selectivity of 98%.



## 1. Introduction

In recent decades, nitrate remediation has been extensively studied due to constantly-rising contamination from anthropogenic origins, e.g. fertilizers, explosives and metal finishing industries, nuclear energy production, etc. The most common treatments for removing $NO_3^-$ ions from contaminated water involve biological [1] and physicochemical methods (e.g. electrodialysis, [2] reverse osmosis, [3] ion exchange resins, [4] and catalytic reduction by hydrogen [5]). The electrochemical conversion of nitrate represents an attractive alternative due to its many advantages over the aforementioned methods, including controlled reaction rate/selectivity, no requirement for chemical additions, and its effectiveness at low cost. Therefore, the electrolytic procedure represents a promising solution for nitrate removal in concentrated solutions present in nuclear waste, among others [6,7].

A wide range of catalytic materials have already been reviewed with regard to efficient denitrification via electrochemical routes, [8] but Pt remains one of the most frequently studied metals for the electroreduction of $NO_3^-$ [7] and $NO_2^-$ [8]. Several studies have been conducted on Pt in acid and neutral solutions, showing that ammonium and nitrous oxide are the primary final products [9,10]. It was recently shown that $HNO_3$ is the only reducible species on Pt. [11] Accordingly, Pt does not exhibit any electrocatalytic activity for the reduction of nitrate in alkaline electrolyte, since $HNO_3$ is deprotonated and the concentration of $HNO_3$ is minimal (as opposed to the concentration of $NO_3^-$, which is maximized). In contrast, Pt is highly active for the reduction of nitrite ($NO_2^-$) in alkaline electrolyte, and it was recently shown that quasi-perfect Pt(100) domains exhibit high activity and selectivity for the reduction of $NO_2^-$ to $N_2$ [12].

In an attempt to identify materials able to convert harmful $NO_3^-$ to harmless $N_2$, one strategy would consist of coupling two different materials, each specifically designed to perform a given reaction with high selectivity. Thus, quasi-perfect Pt(100), which exhibits high selectivity for the conversion of $NO_2^-$ to $N_2$, should be coupled with a material able to perform the first step of this reaction and quantitatively transformed $NO_3^-$ to $NO_2^-$.

It is known from the literature that $NO_3^-$ electroreduction in alkaline solution can proceed on Cu and Cu-based compounds. Indeed, bare Cu electrodes displayed the highest $NO_3^-$ reduction activity among coinage metals [13]. Bouzek et al. [14] and Reyter et al. [15] showed that the first step of the electroreduction of $NO_3^-$ on Cu is the nitrate-to-nitrite conversion. However, the reaction does not end there, and a variety of products other than $NO_2^-$ may be formed. Indeed, the shape of the Cyclic Voltammogram (CV) in the potential region where $NO_3^-$ is reduced, and the distribution of

* Corresponding author.
*E-mail address:* guay@emt.inrs.ca (D. Guay).

http://dx.doi.org/10.1016/j.apcatb.2016.01.043
0926-3373/

products ($NO_2^-$, $NH_2OH$, $NH_4OH$, $N_2$), are critically dependent on the history of the Cu electrode and on its morphology [15–17].

An alternative to such ill-defined electrode material and morphologies, which will impart high selectivity for the nitrate-to-nitrite reduction reaction, is an electrode with a well-defined surface structure. For instance, it was shown that the electroreduction of nitrate in acidic solution is sensitive to the surface structure of both Pt [9,18] and Cu-modified Pt single crystals [19,20]. The highest rate of conversion is observed for a Pt(100) single-crystal electrode modified by a monolayer of Cu adatoms [19]. It was shown that the steps are not the active sites for nitrate reduction [21,22]. In acidic solution, nitrate adsorption and reduction was also studied on Cu(100) and Cu(111) single crystals [23,24]. On Cu(100), the structure formed by the adlayer of nitrate at the electrode surface was observed, as was the interconversion between the nitrate and nitrite adlattices.

Studies of nitrate reduction in alkaline electrolyte are more scant, and a strategy for development of a selective catalyst in alkaline media is missing. Study of the nitrate reduction reaction on Cu-modified Pt(100) single crystals in alkaline electrolyte has been recently reported [25]. Using an electrode with only a fractional Cu monolayer deposited on Pt(100), cyclic voltammetry measurements and online electrochemical mass spectrometry showed that the Cu sites catalyze the reduction of $NO_3^-$ to $NO_2^-$ and $NH_3$ (at two different potentials), while the Pt(100) sites catalyze the reduction of $NO_2^-$ to $N_2$ at a higher potential. However, the current efficiency for the various products ($NO_2^-$ and $NH_3$) could not be obtained due to the low surface area of the Pt single-crystal electrode. Accordingly, it would be highly desirable to study the nitrate reduction reaction on electrodes with well-defined crystallographic surface orientations, but with extended surface areas, so that current efficiency measurements could be determined through standard analytical methods.

We recently showed that Pt nanostructured thin films, $Pt_{NSF}$, with surface roughness, $R_f$, in excess of 400 and with a maximum of 50% of (100) surface sites can be prepared by electrodeposition of a $Pt^{4+}$ salt by carefully controlling deposition conditions [26–30]. $Pt_{NSF}$ is an ideal substrate to study the nitrate reduction reaction, since (i) bare Pt does not exhibit any electrocatalytic activity for the nitrate reduction reaction, and thus the background current will be negligible, (ii) the surface of $Pt_{NSF}$ and the electrocatalytic activity of the electrode can be modified by adatoms through irreversible adsorption (of Bi [31,32] and Sb [32,33]), or by electrodeposition of a fraction of, or up to a monolayer of, an adatom (Pd [32]).

In the following, $Pt_{NSF}$ with extended surface area and a large fraction of (100) surface sites will be modified by a Cu monolayer through underpotential deposition, $Cu_{upd}$. A full analysis of the $Cu_{upd}$ stripping peaks, through deconvolution of the voltammetric profiles, will show that the Cu monolayer adopts the crystallographic orientation of the underlying substrate, i.e. a pseudomorphic Cu overlayer has been deposited on the surface of the substrate. The electrocatalytic activity for $NO_3^-$ reduction will be assessed and a detailed analysis of the products formed in alkaline solution will be conducted. It will be shown that the nitrate reduction reaction is structure-sensitive and occurs predominantly at Cu(100) surface sites, where the current efficiency of the nitrate-to-nitrite conversion is higher than 95%.

## 2. Experimental

### 2.1. Catalyst preparation

Platinum thin films were prepared by electrodeposition on titanium foil (Alfa Aesar, 99%, 0.2 mm thick) pretreated as described elsewhere [28]. The electroplating solution consisted of 10 mM HCl (Fisher Scientific, ACS) and 0.5 mM $Na_2PtCl_6{\cdot}6H_2O$ (Alfa Aesar). Potentiostatic deposition was performed using a Solartron SI 1287 potentiostat, with a $Hg/HgSO_4$ and Pt gauze as reference and counter electrodes, respectively. Since experiments were carried out in both acidic and alkaline media, all potentials mentioned below have been converted and refer to a reversible hydrogen electrode (RHE) *viz.* $V_{vsRHE} = V_{vsHg/HgSO4} + 0.715 + 0.059{*}pH$. Solution resistance was measured through the current interrupt technique and used to correct the value of the working potential. The applied deposition potentials, $E_d$, were $E_d$ = +0.10 V, 0.00 V, −0.05 V and −0.10 V and the films prepared at these different deposition potentials were denoted $Pt_{pc}$, $Pt_{NSF}$/0.00 V, $Pt_{NSF}$/-0.05 V and $Pt_{NSF}$/-0.10 V respectively, since it was shown elsewhere that polycrystalline Pt is obtained at $E_d$ = +0.10 V, while a preferentially (100)-oriented Pt film is obtained at $E_d$ = 0.00 V, −0.05 V and −0.10 V [27–29,]. In all cases, the deposition charge was adjusted to obtain a roughness factor, $R_f$, of *ca.* 30, with $R_f$ defined as the ratio between the electroactive surface area (see below) and the geometric surface area. After deposition, the Pt electrodeposits were thoroughly rinsed with and stored in deionized water (>18.2 MΩ $cm^{-1}$, Millipore, Milli-Q gradient). Further electrochemical experiments were carried out with a Biologic VSP potentiostat. Cyclic voltammetry experiments were carried out in 0.5 M $H_2SO_4$ electrolyte (Merck, Omnitrace, high purity) in a three-compartment glass cell at room temperature. The electrolyte was purged with argon (N5.0, Praxair) for 30 min prior to any electrochemical procedure. An argon flow was continuously maintained over the solution during the electrochemical analysis. Pt deposits were first activated by potential cycling between 0.04 V and 0.82 V at 50 mV $s^{-1}$ to obtain stable voltammetric profiles. The ElectroActive Surface Area (EASA, $cm^2_{Pt}$) of each deposit was evaluated from the $H_{upd}$ charge calculated from stable CV between 0.08 V and 0.45 V, corrected for the double layer charging current and using a conversion factor of 210 μC $cm^{-2}_{Pt}$ [34].

Underpotential deposition of copper on the Pt surface, designed as $Cu_{upd}$/Pt, was carried out in 0.5 M $H_2SO_4$ + 2 mM $CuSO_4{\cdot}5H_2O$ (Sigma-Aldrich, Reagent Plus) electrolyte. The deposition conditions will be detailed later. For comparison purposes, bulk Cu films were deposited at +0.05 V over 45 min. These later films were denoted $Cu_{bulk}$/Pt.

After electrodeposition of Cu in 0.5 M $H_2SO_4$ + 2 mM $CuSO_4$, the electrode was removed from the electrolyte while the electrode potential was maintained at the desired value (see details later on). The electrode was rapidly (within a minute) transferred into the 0.1 M NaOH electrolyte without rinsing. The immersion of the electrode in 0.1 M NaOH was also performed under potential control (*ca.* 0.0 V vs RHE).

#### 2.1.1. Electrochemical measurements

Prior to any electrochemical measurements, all glassware was cleaned in sulfochromic acid for 24 h and rinsed extensively with deionized water. Cyclic voltammetry experiments were carried out in 0.1 M NaOH electrolyte (NaOH 99.9% pellets, ACS, Fisher Scientific) at different nitrate concentrations ranging from 0 to 0.08 M $NaNO_3$ (Fisher Scientific, BioReagent). Potentiostatic electrolyses were performed at +0.10 V and −0.10 V in 0.1 M NaOH + 0.1 M $NaNO_3$ (pH 13) aqueous solutions. A three-compartment cell with a Nafion® membrane (Ion Paul Inc.; Membrane N117, 183 μm thick) was used to separate the working and counter electrode compartments and to prevent the re-oxidation of reduced $NO_3^-$ products. Prior to electrolysis, dissolved oxygen was removed from the solution by bubbling with high-purity argon for 30 min.

#### 2.1.2. Product quantification

Gas chromatograph (GC, Agilent technologies 490 Micro GC) was used at the end of each electrolysis experiment (*ca.* 30 min)

for the quantification of $H_2$, the only major gas-phase product. The concentration of $NO_3^-$ and $NO_2^-$ anions were measured by an ion chromatograph (Dionex 1500) equipped with a Dionex Ion Pac AS9-HC anion exchange column and a chemical suppressor (ASR-ultra 4 mm), using 1 mM $NaHCO_3$ as eluent at 9 mL $min^{-1}$. The $NH_3$ concentrations were determined by visible spectroscopy (Nessler's method) on a Varian spectrometer (Cary-1E). The presence of hydrazine (ASTM standard D1385, "Test Method for Hydrazine in Water") was assessed using visible spectroscopy, but hydrazine concentration was below the detection limit. As shown elsewhere, hydroxylamine is not detected in the reaction products formed during nitrate reduction in 0.1 M $NaNO_3$ + 1 M NaOH solution on copper electrode even if linear scan voltammetry at different scan rates suggest its formation [15]. Since hydroxylamine is chemically stable in the absence of oxygen in alkaline conditions, this is thought to arise because it is only an intermediate product and is readily reduced to ammonia [15].

The total faradic efficiency (FE) was calculated by determining the number of coulombs associated with the formation of each product and the total charge passed during the nitrate reduction process. The average value of the total FE was 91 ± 8% (standard deviation). The fact that this value is slightly lower than 100% is attributed to $H_2$ loss to the atmosphere during the insertion and withdrawal of the needle used to sample the gas over the solution. These losses accumulate at each sampling. This effect is most particularly evident in the case of $Pt_{NSF}$ tested in 0.1 M NaOH and in the absence of $NaNO_3$. In that case, hydrogen evolution is the only reaction occurring at the electrode and five samplings ought to be carried out, due to the large amount of evolved hydrogen. In that case, the total FE was only 81%. To support the comparisons between the various catalysts, and since no products other than hydrogen, nitrate, nitrite and ammonia were detected, the total FEs were normalized to 100%.

#### 2.1.3. Physico-chemical characterization

Scanning Electron Microscopy (SEM) images of the electrodes were taken with JEOL (JSM) equipment.

## 3. Results and discussion

### 3.1. Determination of the deposition conditions of $Cu_{upd}$ at $Pt_{NSF6300F}$

As shown elsewhere, $Pt_{NSF}$ has a very porous structure with pores of a few micrometers diameter [27]. CV of $Pt_{NSF}$/-0.1 V were carried out at 2 mV $s^{-1}$ in 0.5 M $H_2SO_4$ (dotted curve in Fig. 1) and in 0.5 M $H_2SO_4$ + 2 mM $CuSO_4$ (solid curve in Fig. 1) to assess the optimal conditions (primarily deposition potential and deposition time) for obtaining a full monolayer of Cu through underpotential deposition, $Cu_{upd}$, over the whole accessible surface of $Pt_{NSF}$,

CV for $Pt_{NSF}$/-0.1 V in $H_2SO_4$ (inset of Fig. 1) shows the typical hydrogen desorption features for preferentially (100) oriented Pt surfaces, as previously described: [27,28,30,35–37] $h_1$ peak at ca. 0.125 V related to (110) step sites; $h_2$ at ca. 0.270 V attributed to (100) step sites; $h_3$ at ca. 0.340 V related to (100) terraces; and finally, $h_4$ at ca. 0.470 V attributed to the adsorption of (bi-) sulfates on (111) terraces. In presence of $CuSO_4$ (solid curve in Fig. 1), underpotential deposition of copper is observed from 0.80 V to 0.40 V during the reverse potential sweep. Cathodic current shoulders are observed at ca. 0.67, 0.60 and 0.56 V related to $Cu_{upd}$ onto different specific Pt surface sites, in close agreement with previous reports [9,38,39–41]. Below 0.40 V, bulk deposition of copper occurs and the current reaches a diffusion-limited regime at potential below 0.20 V. During the positive potential sweep, bulk copper film oxidation extends from 0.20 V to 0.45 V and is characterized by a huge current peak. Above 0.45 V, $Cu_{upd}$ monolayer stripping is observed, giving rise to several specific features (peaks and shoulders), which will be discussed in detail below. From this experiment, it can be estimated that the lower potential value for the electrodeposition of a full $Cu_{upd}$ monolayer at $Pt_{NSF}$ surfaces is 0.4 V. This value is in agreement with the standard reversible potential of the $Cu^{2+}$/Cu redox couple [42].

To assess the Cu coverage onto the $Pt_{NSF}$ surface, the $Cu_{upd}$ stripping charge, $Q_{Cuupd}$, was measured and compared to the $H_{upd}$ desorption charge, $Q_{Hupd}$, measured in copper-free $H_2SO_4$ solution (cf. shaded areas in Fig. S1). It is well-known that the charge corresponding to the stripping of a monolayer of Cu adatoms should be twice as large as the charge for desorption of H atoms, since both Cu and H atoms are sharing the same adsorption site and two electrons are exchanged during oxidation of one Cu atom, compared to one for H atoms [43,44]. Accordingly, the Cu monolayer coverage, expressed as a percentage, is given by $Q_{Cuupd}/2\ Q_{Hupd}$. As seen in Fig. S2, percent coverage of Cu is very close to 100% for $E_d$ = 0.36 and 0.38 V and for $t_d$ larger than 0.5 h, indicating that a full monolayer of Cu has been deposited at the surface of the $Pt_{NSF}$ electrode in these conditions. For $E_d$ = 0.31 V, percent coverage of Cu is *ca.* 170%, indicating that more than one monolayer of Cu has been deposited. In this case, percent coverage of Cu also increased slightly with deposition time, which is expected when bulk Cu deposition is occurring. In the following, the parameters for the deposition of a full $Cu_{upd}$ monolayer onto $Pt_{NSF}$ were fixed at $E_{dep}$ = 0.38 V and $t_d$ = 150 min. As seen in Fig. S3, the CV in copper-free $H_2SO_4$ solution of a $Pt_{NSF}$ electrode, after it was used several times as a substrate for the deposition and stripping of a Cu monolayer, is almost identical to that of the as-prepared electrode, indicating that the surface crystallographic orientation was maintained throughout the process. This is consistent with the fact that surface re-organization of the $Pt_{NSF}$ electrode does not occur before the potential reaches the region where Pt oxide formation/reduction occurs [27,31,33]. As shown in Fig. S4, there is no modification of the $Pt_{NSF}$ film's surface morphology upon deposition of either a Cu monolayer or a thin Cu bulk film.

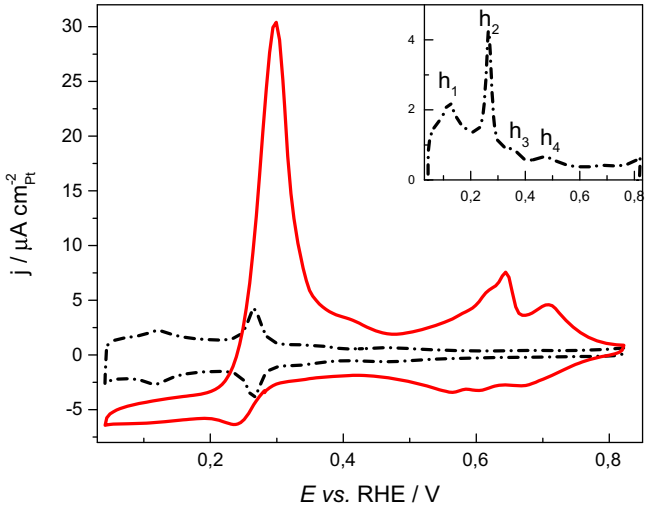


**Fig. 1.** Cyclic voltammetries (2 mV $s^{-1}$) for electrodeposited $Pt_{NSF}$/−0.10 V surfaces in 0.5 M $H_2SO_4$ (black dotted curve) and in 2 mM $CuSO_4$+ 0.5 M $H_2SO_4$ (red curve). For clarity, a magnification of the $H_{upd}$ desorption potential range is shown in the inset. (For interpretation of the references to colour in this figure legend, the reader is referred to the web version of this article).

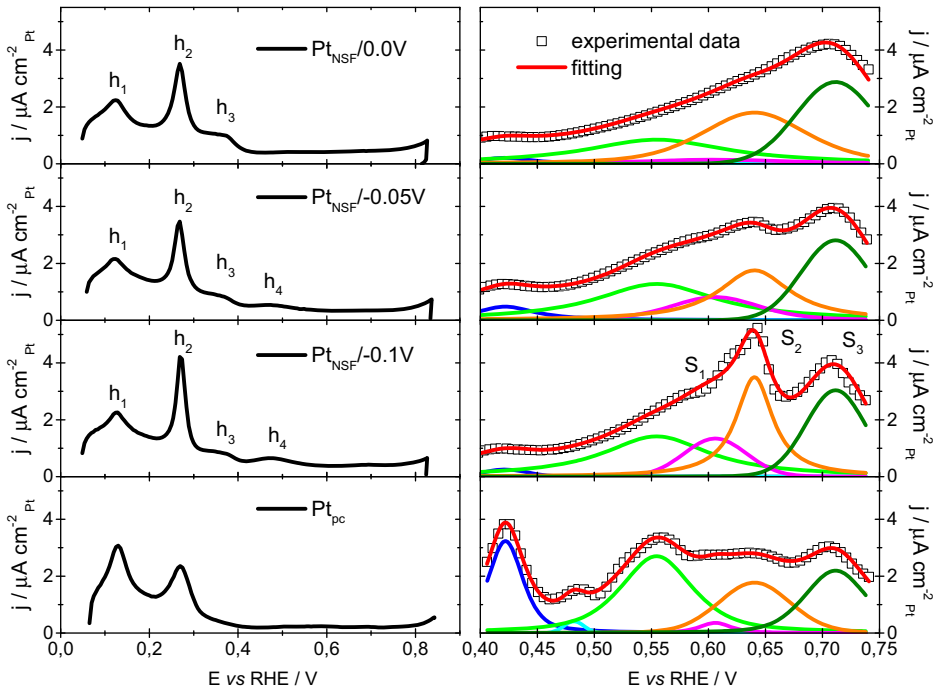


**Fig. 2.** Linear potential sweeps (2 mV $s^{-1}$) in 0.5 M $H_2SO_4$ for electrodeposited Pt films (left panels) and for corresponding Cu stripping curves from $Cu_{upd}$/Pt surfaces (right panels). Refer to the text for additional details.

### 3.2. *Identification of crystallographic surface domains by $Cu_{upd}$ stripping at $Pt_{NSF}$*

Underpotential deposition of Cu was performed on the various $Pt_{pc}$ and $Pt_{NSF}$ films under study. Before examining the details of that study, it is worthwhile to summarize what is known about these Pt films and how the deposition potential affects their microstructure.

It was shown elsewhere that the surface crystallographic orientation of $Pt_{NSF}$ films could be tuned by adjusting the deposition potential [28]. In summary, Pt films show a preferential orientation along the (100) axis for $-0.10 \leq E_{dep} \leq 0.00$ V. In that range of deposition potentials, a constant proportion of (100) sites (*ca.* 40%) is observed, but the fraction of (100) terraces decreases from 45% to 25%, while that of (100) steps increases from 55% to 75%, as $E_{dep}$ is varied from the upper to the lower potential limit. At the same time, the proportion of (111) sites is increased from *ca.* 3% to 19% when $E_{dep}$ varied from 0.00 V to −0.10 V [28]. This is nicely illustrated by looking at the CV of the various $Pt_{NSF}$ films taken in 0.5 M $H_2SO_4$ and depicted in Fig. 2. The intensity of peak $h_3$ corresponding to (100) terraces decreases continuously as $E_{dep}$ is varied from 0.00 to −0.10 V, while $h_2$ (100 steps) and $h_4$ (111 sites) contributions are increased. As mentioned earlier, Pt deposited at $E_{dep}$ > 0.00 V exhibit a CV characteristic of polycrystalline Pt.

Using the deposition conditions defined above, $Cu_{upd}$ was performed on both $Pt_{pc}$ and $Pt_{NSF}$ films. As seen in the right panel of Fig. 2, huge differences between the $Cu_{upd}$ stripping curves of these four Pt films are observed. These differences reflect a modification of the surface crystallographic orientations of the underlying $Pt_{NSF}$ film with the deposition potential. As a first qualitative analysis, it is worth focusing on the last three stripping peaks: $S_1$ (0.60 V), $S_2$ (0.64 V) and $S_3$ (0.70 V). Extensive studies have already been performed on the $Cu_{upd}$ processes occurring at low index plane of Pt single crystal electrodes [45]. However, the study of Cu underpotential deposition on Pt stepped surfaces may represent a more suitable comparison with the complex nanostructured surfaces under study here. For example, Nishira and Nozoye [40] demonstrated that the stripping peaks for Cu adatoms on Pt(111) terraces and Pt(100) steps occurs at *ca.* 0.60 V and 0.66 V, respectively. These potential values closely correspond to $S_1$ and $S_2$ peaks in Fig. 2. In another study, Francke et al. [41] demonstrated that the $Cu_{upd}$ adsorption strength at Pt(100) terraces is larger than at Pt(111) steps. Cu stripping from such Pt(100) terraces is observed at *ca.* 0.75 V (at 50 mV$s^{-1}$). Therefore, peak $S_3$ at 0.70 V is assigned to the $Cu_{upd}$ stripping from Pt(100) terraces, the lower potential value for $S_3$ being attributed to the slower sweep rate used in the present study (2 mV $s^{-1}$).

Comparison of the $Cu_{upd}$ and $H_{upd}$ stripping curves for the different Pt electrodeposits in Fig. 2 confirms this qualitative analysis. Indeed, while CV in $H_2SO_4$ for a $Pt_{NSF}$/0.00 V exhibits a higher proportion of (100) terraces (peak $h_3$), the corresponding $Cu_{upd}$ stripping curve is dominated by peak $S_3$ at *ca.* 0.70 V, attributed to (100) terraces. In comparison, CV in $H_2SO_4$ for $Pt_{NSF}$/-0.10 V shows higher currents for $h_2$ and $h_4$, *i.e.* More (100) step sites and (111) terraces respectively, with corresponding higher currents for $S_1$ and $S_2$ in the Cu stripping curves related to (111) terraces and (100) step sites, respectively.

In order to obtain more quantitative results on the influence of the Pt surface crystallographic orientations on the Cu stripping features, deconvolution of the $Cu_{upd}$ stripping curves was carried out. In addition to the three features ($S_1$, $S_2$ and $S_3$) already discussed, three additional peaks may be distinguished in the Cu stripping curves of Fig. 2 at *ca.* 0.42 V, 0.48 V and 0.56 V. These additional peaks are all attributed to Cu adatoms on (110) sites and default sites on the basis of the work of Buller et al. who showed that $Cu_{upd}$ stripping from Pt(110) sites occurred between 0.40 V and 0.55 V, at lower potentials than on (111) terraces, (100) steps and (100) terraces [39]. Accordingly, each of the four Cu stripping curves of Fig. 2 were fitted using six different components. The positions of each single component ($xc_1$, $xc_2$, $xc_3$, $xc_4$, $xc_5$ and $xc_6$, where $xc_i$ is the peak center of the ith component) were shared between the four Cu stripping curves (the $xc_i$'s of each individual cu stripping curves are the same). The fitted curves are displayed in the right panels of Fig. 2 (red solid lines). The fit with the experimental data (open squares)

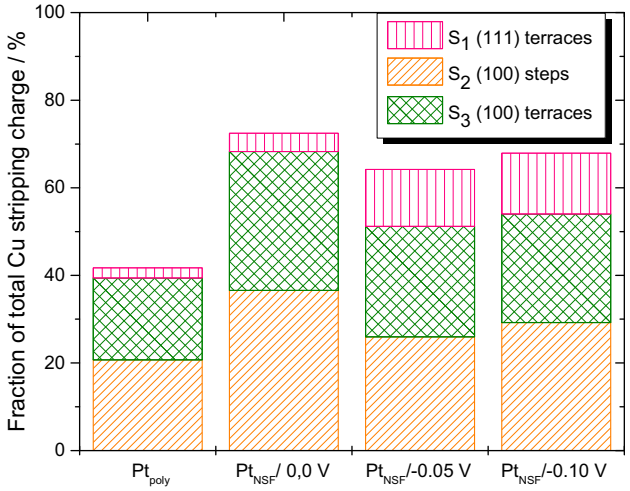


**Fig. 3.** Relative proportion of the $S_1$ (0.60 V), $S_2$ (0.66 V) and $S_3$ (0.70 V) Cu components in the $Cu_{upd}$ stripping curves for various Pt films.

is excellent. The ratio $A_p/\Sigma(A_p)$, where $A_p$ is the area of one peak, was used to estimate the fraction of the surface sites occupied by one particular Cu atom. Fig. 3 shows the fraction of total stripping charges under the peaks $S_1$, $S_2$ and $S_3$ for the various films studied here. In the case of $Pt_{NSF}$ films, $S_1 + S_2 + S_3$ accounts for close to 70% of the Cu contributions, compared to 40% in the case of $Pt_{pc}$ (*cf.* Fig. S5 for full quantification of the various contributions). Indeed, all the $Pt_{NSF}$ films present a total fraction of (100) sites ($S_2 + S_3$) ranging from 50% to 70%, while this fraction remains below 40% for $Pt_{pc}$. $S_3$ reached a maximum value of *ca.* 32% for $Pt_{NSF}$/0.00 V, which is consistent with the intensity of peak $h_3$ observed in 0.5 M $H_2SO_4$ and attributed to (100) terrace atoms (Fig. 2). Finally, $S_1$ (0.60 V) is significantly present (*ca.* 15% of total surface sites) only in $Pt_{NSF}$/-0.05 V and $Pt_{NSF}$/-0.10 V, which agrees well with the fact that the current peak ($h_4$) observed at 0.47 V in 0.5 M $H_2SO_4$ and attributed to the adsorption of (bi-) sulfates on (111) terraces is observed exclusively in the case of $Pt_{NSF}$/-0.05 V and $Pt_{NSF}$/-0.10 V. Interestingly, it is seen in Fig. S6 that a very small change in the $h_4$ current peak resulted in a much larger change in component $S_1$ of the corresponding Cu stripping curves, which confirms the previous assignment.

### 3.3. Selective $Cu_{upd}$ stripping

A potentiostatic technique was used to partially and selectively oxidize a fraction of the Cu monolayer. Thus, following deposition of a full Cu monolayer, the electrode potential was set to different stripping potentials ($E_{strip}$) between 0.37 and 0.66 V. The stripping potential was maintained until a steady-state current close to zero was reached to selectively remove part of the Cu monolayer. The potential was then scanned from $E_{strip}$ up to 0.78 V to remove the portion of the Cu monolayer not removed at $E_{strip}$. The procedure was repeated by depositing a new Cu monolayer and increasing $E_{strip}$. A few representative Cu stripping curves for $Pt_{NSF}$/-0.10 V are shown in Fig. 4 for various values of $E_{strip}$.

In all cases, the Cu stripping curves recorded from $E_{strip}$ to 0.78 V have the same shape and nearly the same current intensity as the one recorded from $E_{strip}$ = 0.37 V to 0.78 V (stripping of a full monolayer). This indicates that migration of Cu atoms from an occupied site to an unoccupied one does not occur to any significant extent on the experiment's time scale (otherwise, the shape and the current intensity of the two curves in the potential region extending from $E_{strip}$ to 0.78 V would be different). Focusing on the curve with $E_{strip}$ = 0.60 V, the charge associated with oxidation of the Cu atoms still adsorbed at the surface of $Pt_{NSF}$/-0.10 V represents 59% of the stripping charge of a full monolayer, indicating the remaining Cu atoms still covered 59% of the underlying Pt substrate. As previously noted in Fig. 2, only (100) step and (100) terrace sites display $Cu_{upd}$ oxidation at potentials higher than 0.60 V. It may be concluded that (100) sites represents 59% of the surface, which is consistent but slightly higher than previously observed by deconvolution of the stripping peaks (Fig. 2). This might be due to the shape of the peak (a mix of Gaussian and Lorentzian functions) used in the deconvolution procedure, which may lead to overestimating the most prominent species. The 59% value for the (100) step and (100) terrace sites determined by selective $Cu_{upd}$ stripping is also higher than the value determined by the $H_{upd}$ deconvolution method, which results in a value closer to 50% [28]. In the $H_{upd}$ deconvolution process, only three peaks (at 0.270 V, 0.338 V and 0.369 V) are associated with (100) ordered domains and are taken into account in the evaluation of the (100) step and (100) terrace sites. However, the (100) step sites near (111) terraces result in a peak at 0.256 V, [37] and this contribution is not taken into account when evaluating (100) step and (100) terrace sites. It is hypothesized that Cu stripping from these (100) step sites near (111) terraces is occurring at a potential larger than 0.60 V. Such an event would result in a systematic increase of the apparent amount of (100) sites by the selective Cu stripping method, as compared to the hydrogen deconvolution method.

Using selective stripping, it is thus possible to prepare high surface area catalysts with controlled composition and crystallographic surface orientations. In the following, the deposition of a full Cu monolayer at the surface of $Pt_{NSF}$/-0.10 V followed by partial stripping ($E_{strip}$ = 0.60 V) will be used to prepare electrodes with Cu atoms exclusively adsorbed at (100) surface sites. Hereafter, these electrodes will be denoted indistinctively as $Cu_{upd}/Pt_{NSF}$ (~0.6 ML) or $Cu_{100}/Pt_{NSF}$ to emphasize this fact.

### 3.4. Electrochemical performance of $Cu_{upd}/Pt_{NSF}$ electrodes for nitrate reduction

Linear sweep voltammetry (LSV) was first carried out in 0.1 M NaOH + $NaNO_3$ (from 0 to 0.08 M) in order to provide a qualitative assessment of the various electrodes' catalytic performance. In each case, the fifth consecutive LSV curve at each $NO_3^-$ concentration will be used. As shown in Fig. S4, the deposition of

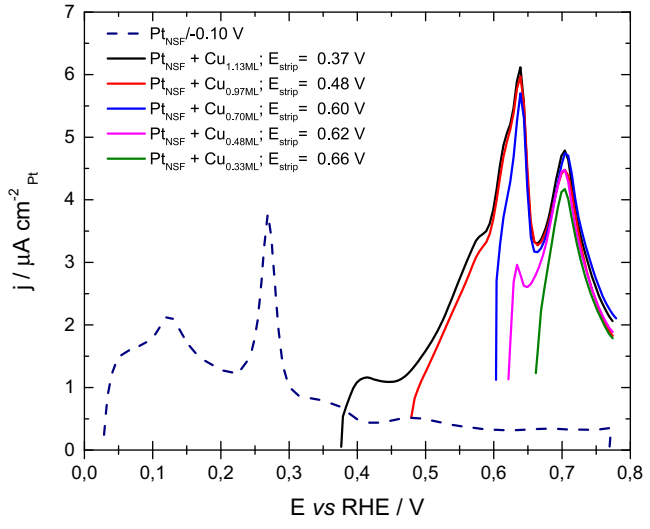


**Fig. 4.** Linear potential sweeps (2 mV $s^{-1}$) in 0.5 M $H_2SO_4$ for $Pt_{NSF}$/−0.10 V (dotted line) and for corresponding $Cu_{upd}$ stripping curves, taken from different values of $E_{strip}$. Colored lines are used for different $E_{strip}$ values, leading to different Cu coverages. For additional details, please refer to the text.

copper in the form of a monolayer ($Cu_{upd}/Pt_{NSF}$ −0.10 V) or a thin bulk layer ($Cu_{bulk}/Pt_{NSF}$ −0.10 V) does not change the morphology of the electrode and thus does not affect its EASA. The negative sweeps for $Pt_{NSF}$, $Cu_{bulk}/Pt_{NSF}$, $Cu_{upd}/Pt_{NSF}$ (1 ML) and $Cu_{upd}/Pt_{NSF}$ (~0.6 ML) are presented in Fig. 5A, 5B, 5C and 5D, respectively. Without nitrates in solution (solid black lines), $Pt_{NSF}$ exhibits large currents at potentials lower than 0.0 V due to the hydrogen evolution reaction (HER). In comparison, $Cu_{bulk}/Pt_{NSF}$ shows very poor HER activity (black curve in Fig, 5B), which is expected for a Cu surface. The activity of $Cu_{upd}/Pt_{NSF}$ (1 ML) for the HER is similar but slightly higher to what is observed for $Cu_{bulk}/Pt_{NSF,}$ while that of $Cu_{upd}/Pt_{NSF}$ (~0.6 ML) is more comparable to $Pt_{NSF}$. Since it was previously demonstrated that the surface of the $Cu_{upd}/Pt_{NSF}$ (1 ML) electrode was entirely covered with a Cu monolayer, its low activity for the HER is as expected. The slightly higher activity for the HER compared to $Cu_{bulk}/Pt_{NSF}$ might be due to an electronic effect of the $Pt_{NSF}$ substrate on the Cu monolayer [46–48]. Additional study will be needed to ascertain this phenomenon. The current of $Cu_{upd}/Pt_{NSF}$ (~0.6 ML) for the HER is very similar to bare $Pt_{NSF}$ because Cu atoms cover only a fraction of the electrode surface and a large amount of Pt atoms are exposed to the electrolyte.

Upon addition of $NaNO_3$, the CV for $Pt_{NSF}$ (Fig. 5A) remains virtually unchanged. This is consistent with the literature, since it is known that the reduction of nitrate at Pt surface is pH sensitive and does not occur in alkaline electrolyte [11]. In the case of $Cu_{upd}/Pt_{NSF}$ (1 ML) (Fig. 5C), the LSV curve in presence of $NaNO_3$ exhibits a clearly discernible peak at +0.15 V, along with an increased current density at lower potential. The intensity of this peak increases upon further addition of nitrates, as does the current at lower potential. It will be shown later on that the current peak at +0.15 V corresponds to the reduction of nitrate to nitrite. It occurs at a potential which is 150 mV before the $H_2/H_2O$ reversible potential. This peak is not observed in the LSV curves of $Cu_{bulk}/Pt_{NSF}$ (Fig. 5B). These later curves only show a small shoulder at +0.15 V, indicating that the nitrate-to-nitrite reduction is occurring at a much smaller rate. Later in this study, we will determine that this phenomenon is due to more difficult nitrate adsorption/reduction on the disordered $Cu_{bulk}/Pt_{NSF}$ as opposed to the well-structured and pseudomorphic copper atomic arrangement on $Cu_{upd}/Pt_{NSF}$. On $Cu_{bulk}/Pt_{NSF}$, the main feature is observed at −0.10 V, where a larger current peak is observed on the curves obtained by subtracting the LSV curves recorded in presence of $NaNO_3$ from the blank curve ($[NaNO_3] = 0.0$ M) (see Fig. S7). In the case of $Cu_{upd}/Pt_{NSF}$ (~0.6 ML) (Fig. 5D), there is also a very discernible peak at +0.15 V. The intensity of that peak is almost identical to that of $Cu_{upd}/Pt_{NSF}$ (Fig. 5C) despite Cu atoms from (110) and (111) surface sites being dissolved. This is a strong indication that the reduction of nitrate is occurring on Cu(100) surface sites, since copper atoms only occupy these sites and the exposed Pt surface atoms are inactive for nitrate reduction. Long-term electrolysis experiments (below) will confirm that the activities of both $Cu_{upd}/Pt_{NSF}$ (1 ML) and $Cu_{upd}/Pt_{NSF}$ (0.6 ML) for nitrate-to-nitrite reduction are almost identical. On $Cu_{upd}/Pt_{NSF}$ (0.6 ML), the current peak attributed to the nitrate-to-nitrite reduction is superimposed on a large background current that starts at potential as low as +0.25 V. The peak at +0.25 V is not observed on $Cu_{upd}/Pt_{NSF}$ and $Cu_{bulk}/Pt_{NSF}$. In a series of independent experiments (data not shown), a peak is observed at the same potential on the LSV curves of $Pt_{NSF}$ in 0.1 M NaOH + 0.08 M $NaNO_2$. Accordingly, the current peak observed at +0.25 V on $Cu_{upd}/Pt_{NSF}$ (0.6 ML) in the presence of nitrate (Fig. 5D) is attributed to the reduction of nitrites on the exposed Pt atoms that accumulate in the double layer over the successive LSV curves recorded at each $NO_3^-$ concentration.

In Fig. 5C, the peak current at +0.15 V increases with the $NO_3^-$ concentration. It was shown elsewhere that the reduction current of that peak is linearly dependent on the scan rate, suggesting the process is purely surface-limited, and that adsorption of $NO_3^-$ at the surface of Cu is at equilibrium at the electrode solution interface [17]. Assuming there is no lateral interaction between the adsorbed species, the equilibrium adsorption constant, $b$, can be determined by the Langmuir equation [49]

$$\theta = bc_{NO_3^-}/(1+bc_{NO_3^-}) \quad (1)$$

where $\theta$ is the fractional occupancy of the adsorption sites, and $c_{NO_3^-}$ is the concentration of $NO_3^-$ in solution. Here, $\theta$ is the ratio of the surface concentration of $NO_3^-$ at concentration $c$, $\Gamma$, to its maximum surface concentration, $\Gamma_{max.}$

$$\theta = \Gamma/\Gamma_{max} \quad (2)$$

Then:

$$c_{NO_3^-}/\Gamma = 1/(b\Gamma_{max}) + c_{NO_3^-}/\Gamma_{max} \quad (3)$$

Considering that the reduction current density at +0.15 V is proportional to the surface concentration of nitrate ions, this latter equation can be written:

$$c_{NO_3^-}/j_{+0.15V} = 1/(bj_{max}) + c_{NO_3^-}/j_{max} \quad (4)$$

Plots of $c_{NO_3^-}/j_{+0.15V}$ as a function of $c_{NO_3^-}$ for $Cu_{upd}/Pt_{NSF}$ and $Cu_{bulk}/Pt_{NSF}$ (Fig. S8) show good linearity, with a correlation coefficient close to 0.99. From the intercept and the slope, the adsorption equilibrium constant and $j_{max}$ may be obtained.

The Langmuir constant of $Cu_{upd}/Pt_{NSF}$ is $11.02 \pm 0.35\ M^{-1}$, while that of $Cu_{bulk}/Pt_{NSF}$ is $6.45 \pm 0.54\ M^{-1}$. Unfortunately, a similar analysis could not be conducted on $Cu_{upd}/Pt_{NSF}$ (0.6 ML) due to the reduction of nitrites at Pt surface sites that gave rise to a current peak at +0.25 V. The reciprocal of the Langmuir constant, $b^{-1}$, is the $NO_3^-$ concentration at which $\theta = 0.5$. Therefore, the adsorption of

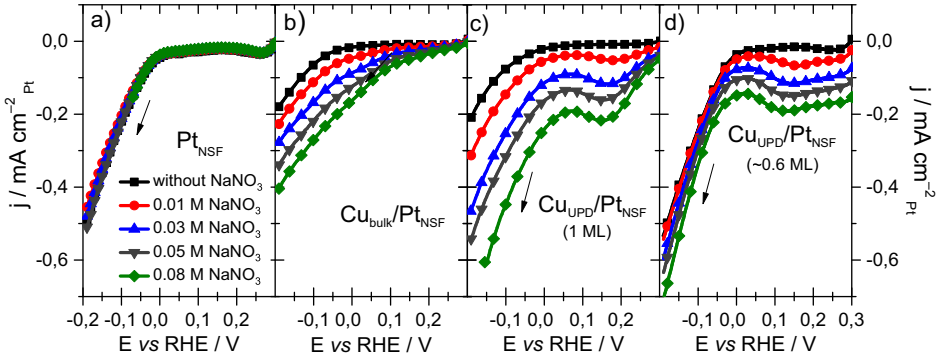


**Fig. 5.** Linear sweep voltammetry in 0.1 M NaOH (50 mV $s^{-1}$) in presence of $NaNO_3$ at (a) $Pt_{NSF}$, (b) $Cu_{bulk}/Pt_{NSF}$, (c) $Cu_{upd}/Pt_{NSF}$ (1 ML) and (d) $Cu_{upd}/Pt_{NSF}$ (~0.6 ML) surfaces. The $NaNO_3$ concentrations are given in panel (a). The fifth consecutive LSV curve is shown at each $NaNO_3$ concentration.

$NO_3^-$ on $Cu_{upd}/Pt_{NSF}$ is facilitated as compared to $Cu_{bulk}/Pt_{NSF}$. The Langmuir constant for $Cu_{upd}/Pt_{NSF}$ is also greater than on a series of Cu electrodes activated by creating a nanostructured surface [17]. In the latter case, the Langmuir constant varies from 1.8 to 3.5 $M^{-1}$ depending on the electrochemical treatment applied to the Cu electrode. Therefore, the presence of a well-organized surface structure is a more important factor in favoring the adsorption of $NO_3^-$ than the formation of a nanostructured surface. Since the current peak at +0.15 V is observed at the same position and nearly the same intensity in the LSV curves of both $Cu_{upd}/Pt_{NSF}$ (1 ML) and $Cu_{upd}/Pt_{NSF}$ (0.6 ML), it is suggested that nitrate is preferentially adsorbed at the Cu(100) surface sites of the electrode.

The $j_{max}$ value of $Cu_{upd}/Pt_{NSF}$ is $0.444 \pm 0.005$ mA $cm^{-2}{}_{Pt}$, while that of $Cu_{bulk}/Pt_{NSF}$ is $0.118 \pm 0.003$ mA $cm^{-2}{}_{Pt}$. The maximum current density of a process limited by the adsorption of the reactant is given by

$$j_{max} = nFk\Gamma_{max} \quad (5)$$

where $n = 2$ for the nitrate-to-nitrite reduction, $F$ is the Faraday constant and $k$ is the rate constant for the nitrate-to-nitrite conversion. The fact that the difference between the $j_{max}$ of $Cu_{upd}/Pt_{NSF}$ and $Cu_{bulk}/Pt_{NSF}$ is close to a factor of four indicates that the transfer of electrons ($k$) is facilitated and/or that the maximum $NO_3^-$ surface concentration is larger on a well-structured Cu surface.

The selectivity and activity of the nitrate reduction process were further assessed by measuring the faradaic efficiency and partial current density for the various products. Faradic efficiency measurements were performed in 0.1 M NaOH + 0.1 M $NaNO_3$ at an applied potential of +0.15 V. The products formed were analyzed following after the passing of a total charge of 10 C. As seen in Fig. 6A, the partial current efficiency for nitrite at +0.15 V is highest at 0.180 mA $cm^{-2}{}_{Pt}$ for $Cu_{upd}/Pt_{NSF}$ and only slightly lower at 0.160 mA $cm^{-2}{}_{Pt}$ for $Cu_{100}/Pt_{NSF}$. This confirms that nitrate-to-nitrite reduction occurs on Cu(100) surface sites. In comparison, the partial current density for nitrite on $Cu_{bulk}/Pt_{NSF}$ is only 0.095 mA $cm^{-2}{}_{Pt}$, lower by a factor of nearly two.

This translates into the same high value of faradaic efficiency for nitrite (in excess of 90–95%, see Fig. 6B). In addition to nitrites, a small amount of ammonia was also detected. Considering the nitrate-to-nitrite reduction is a $2e^-$ process, while $8e^-$ are involved in the reduction of nitrate to $NH_3$, this amounts to less than 2 mol% of $NH_3$, indicating that near quantitative nitrate-to-nitrite reduction has occurred.

Following these measurements, we verified the stability of the adlayer by performing a Cu stripping analysis (see Fig. 7). On $Cu_{up}/Pt_{NSF}$, a comparison of the Cu stripping curves before and after electrolysis (10 C) at +0.15 V in 0.1 M NaOH + 0.1 M $NaNO_3^-$ indicated that the Cu surface coverage had decreased slightly from 100% to 87%. Cu atoms from the (110) sites had been lost in the process, as both Cu stripping curves superimposed each other except between 0.3 and 0.5 V. In the presence of nitrate, the Cu adlayer at the $Pt_{NSF}$ electrode surface is much more stable than in the presence of CO, in which case the Cu overlayer changes from a flat to a granular structure, exposing a much larger part of the Pt surface [46]. In alkaline electrolyte, this is most likely related to the lower heat of adsorption of $NO_3^-$ on Pt as compared to CO (indeed, $NO_3^-$ does not adsorb on Pt in alkaline electrolyte [11]) In contrast, for $Cu_{100}/Pt_{NSF}$, the Cu surface coverage is almost identical; however, the two curves have a very distinct shape, indicating that Cu migration and surface re-organization have occurred during the reduction of nitrate. This is most noticeable in the potential region where the characteristic $S_2$ ((100) step) and $S_3$ ((100) terrace) peaks were observed. The intensity of these peaks decreased during the nitrate reduction process, indicating that Cu atoms adsorbed on these sites had migrated to free surface sites, since the Cu surface stays constant. Diffusion of surface Cu atoms from the (100) sites to free (111) and (110)

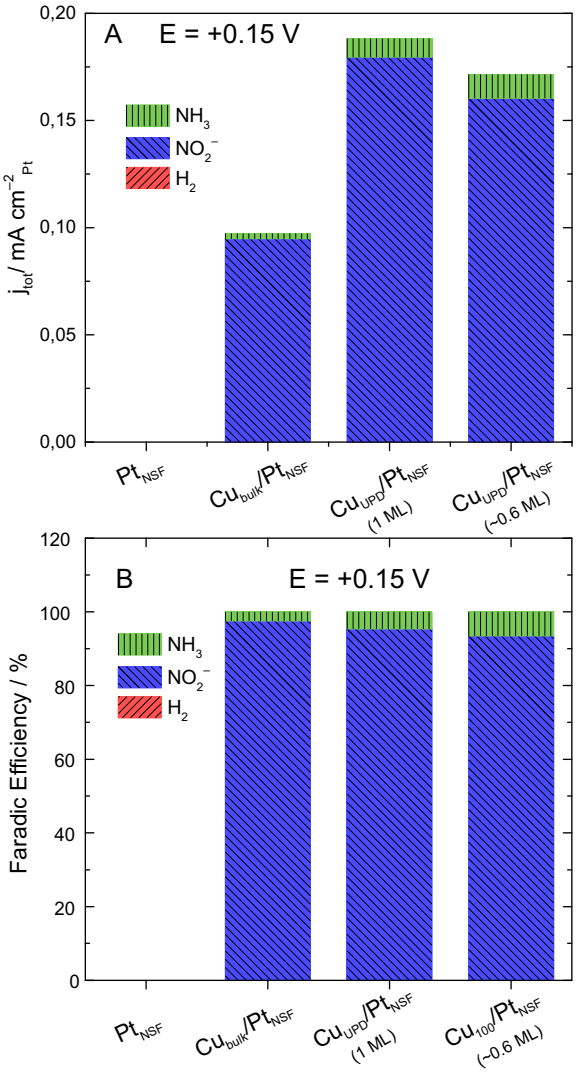


**Fig. 6.** Partial current density (A) and current efficiency (B) for the reduction of nitrate. The electrolyte was 0.1 M NaOH + 0.1 M $NaNO_3$ and the applied potential was +0.15 V. The measurements were carried out after a charge of 10C.

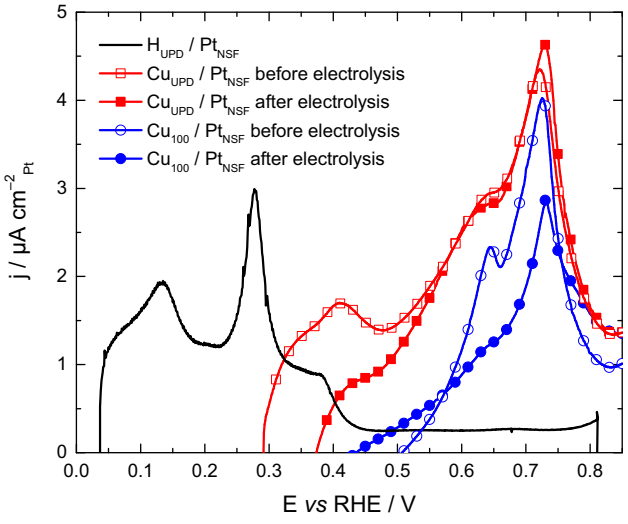


**Fig. 7.** Cu stripping (2 mV $s^{-1}$) in 0.5 M $H_2SO_4$ for $Cu_{upd}/Pt_{NSF}$ 1 ML (red curve) and for $Cu_{100}/Pt_{NSF}$ ~0.6 ML (blue curve), before electrolysis (open symbols) and after electrolysis (filled symbols). (For interpretation of the references to colour in this figure legend, the reader is referred to the web version of this article.)

surface sites is occurring on the time scale of the electrolysis, which ran for *ca.* 40 min. Also, this might explain why the partial current density for nitrite is slightly lower on $Cu_{100}/Pt_{NSF}$ as compared to $Cu_{upd}/Pt_{NSF}$.

## 4. Conclusion

Pt nanostructured thin films $Pt_{NSF}$, with surface roughness $R_f$ in excess of 30, and composed of nearly 50% (100) surface sites were prepared by electrodeposition. These electrodes were used as substrates for underpotential deposition of a Cu monolayer, allowing the ad-layer to adapt the crystallographic surface orientation of the underlying substrate. Subsequent selective stripping of Cu allows Cu atoms to dissolve from specific sites, notably (110) and (111) surface sites, leaving Cu atoms only on the (100) step and terrace surface sites. Using this strategy, we were able to prepare Cu-modified electrodes with both well-defined surface structures and an extended surface area (roughness factor in excess of 30), to quantify products of the nitrate reduction process using standard analytical methods.

It was shown that $NO_3^-$ readily adsorbs on Cu-modified electrodes in alkaline electrolyte. In comparison, $NO_3^-$ does not adsorb on Pt under the same conditions. The adsorption of $NO_3^-$ is favored on $Cu_{upd}/Pt_{NSF}$ ($b = 11.02\ M^{-1}$) as opposed to $Cu_{bulk}/Pt_{NSF}$ ($b = 6.45\ M^{-1}$) and nanostructured Cu electrodes [17]. The maximum current density for the nitrate-to-nitrite reduction increases from $0.12\ mA\ cm^{-2}{}_{Pt}$ for $Cu_{bulk}/Pt_{NSF}$ to $0.48\ mA\ cm^{-2}{}_{Pt}$ for $Cu_{upd}/Pt_{NSF}$. A detailed analysis of the data indicated that this increased activity is mainly due to Cu adsorbed on the (100) surface sites. At +0.15 V *vs* RHE, the nitrate-to-nitrite conversion is almost quantitative, with current efficiency for nitrite above 95% (more than 98 mol% of nitrite), the remainder being $NH_3$. At 100% coverage, the Cu adlayer is quite stable; only 13% of the Cu atoms are lost after prolonged testing for nitrate reduction, and the freed surface sites mostly display (110) characteristics. It would be interesting to combine a $Cu_{upd}/Pt_{NSF}$ electrode, which is highly specific for the nitrate-to-nitrite conversion, with a Pt(100) domain electrode specific to the reduction of nitrite to $N_2$, [50] therefore allowing the two-step conversion of harmful $NO_3^-$ to harmless $N_2$ without generating unwanted by-products.

## Acknowledgements

This work was supported by the Natural Sciences and Engineering Research Council of Canada (NSERC) and the Canada Research Chair program. Moreover, one of the authors (EB) wishes to acknowledge the financial support of the Fonds de Recherche du Québec—Nature et technologies (FRQNT), through the Energy Research Scholarships (A7) program, and that of NSERC, through the Alexander Graham Bell Canada Graduate Scholarship's Doctoral Scholarship.

One of the authors (CR) wishes to acknowledge the financial support of NSERC through its Undergraduate Student Research Awards, and that of FRQNT's Programs of Scholarships of 2nd Cycle.

## Appendix A. Supplementary data

Supplementary data associated with this article can be found, in the online version, at http://dx.doi.org/10.1016/j.apcatb.2016.01.043.

## References

[1] V. Mateju, S. Cizinska, J. Krejci, T. Janoch, Biological water denitrification. A review, Enzyme Microb. Technol. 14 (1992) 170–183.
[2] A. Gherrou, H. Kerdjoudj, R. Molinari, E. Drioli, Removal of silver and copper ions from acidic thiourea solutions with a supported liquid membrane containing D2EHPA as carrier, Sep. Purif. Technol. 28 (2002) 235–244.
[3] J.J. Schoeman, A. Steyn, Nitrate removal with reverse osmosis in a rural area in South Africa, Desalination 155 (2003) 15–26.
[4] A. Kapoor, T. Viraraghavan, Nitrate removal from drinking water—Review, J. Environ. Eng. 123 (1997) 371–380.
[5] W. Gao, N. Guan, J. Chen, X. Guan, R. Jin, H. Zeng, Z. Liu, F. Zhang, Titania supported Pd-Cu bimetallic catalyst for the reduction of nitrate in drinking water, Appl. Catal. B Environ. 46 (2003) 341–351.
[6] J.O. Bockris, J. Kim, Electrochemical treatment of low-level nuclear wastes, J. Appl. Electrochem. 27 (1997) 623–634.
[7] H. Li, D.H. Robertson, J.Q. Chambers, D.T. Hobbs, Electrochemical reduction of nitrate and nitrite in concentrated sodium-hydroxide at platinum and nickel electrodes, J. Electrochem. Soc. 135 (1988) 1154–1158.
[8] M. Duca, M.T.M. Koper, Powering denitrification: the perspectives of electrocatalytic nitrate reduction, Energy Environ. Sci. 5 (2012) 9726–9742.
[9] M.C. Figueiredo, J. Solla-Gulloín, F.J. Vidal-Iglesias, V. Climent, J.M. Feliu, Nitrate reduction at Pt(1 0 0) single crystals and preferentially oriented nanoparticles in neutral media, Catal. Today 202 (2013) 2–11.
[10] S. Taguchi, J.M. Feliu, Kinetic study of nitrate reduction on Pt(110) electrode in perchloric acid solution, Electrochim. Acta 53 (2008) 3626–3634.
[11] J. Yang, P. Sebastian, M. Duca, T. Hoogenboom, M.T.M. Koper, pH dependence of the electroreduction of nitrate on Rh and Pt polycrystalline electrodes, Chem. Commun. 50 (2014) 2148–2151.
[12] T. Chen, H. Li, H. Ma, M.T.M. Koper, Surface modification of Pt(100) for electrocatalytic nitrate reduction to dinitrogen in alkaline solution, Langmuir 31 (2015) 3277–3281.
[13] G.E. Dima, A.C.A. De Vooys, M.T.M. Koper, Electrocatalytic reduction of nitrate at low concentration on coinage and transition-metal electrodes in acid solutions, J. Electroanal. Chem. 554 (2003) 15–23.
[14] K. Bouzek, M. Paidar, A. Sadilkova, H. Bergmann, Electrochemical reductionof nitrate in weakly alkaline solutions, J. Appl. Electrochem. 31 (2001) 1185–1193.
[15] D. Reyter, D. Bélanger, L. Roué, Study of the electroreduction of nitrate on copper in alkaline solution, Electrochim. Acta 53 (2008) 5977–5984.
[16] D. Reyter, G. Chamoulaud, D. Bélanger, L. Roué, Electrocatalytic reduction of nitrate on copper electrodes prepared by high-energy Ball milling, J. Electroanal. Chem. 596 (2006) 13–24.
[17] D. Reyter, M. Odziemkowski, D. Bélanger, L. Roué, Surface characterization electrochemical behavior, and properties for the electroreduction of nitrate, J. Electrochem. Soc. 154 (2007) K36–K44.
[18] S. Taguchi, J.M. Feliu, Kinetic study of nitrate reduction on Pt(110) electrode in perchloric acid solution, Electrochim. Acta 53 (2008) 3626–3634.
[19] A.V. Rudnev, E.B. Molodkina, M.R. Ehrenburg, R.G. Fedorov, A.I. Danilov, Y.M. Polukarov, J.M. Feliu, Methodical aspects of studying the electroreduction of nitrate on modified single crystal Pt(hkl)+Cu electrodes, Russian J. Electrochem. 45 (2009) 1052–1063.
[20] E.B. Molodkina, M.R. Ehrenburg, Y.M. Polukarov, A.I. Danilov, J. Souza-Garcia, J.M. Feliu, Electroreduction of nitrate ions on Pt(1 1 1) electrodes modified by copper adatoms, Electrochim. Acta 56 (2010) 154–165.
[21] E.B. Molodkina, I.G. Botryakova, A.I. Danilova, J. Souza-Garcia, J.M. Feliu, Mechanism of nitrate electroreduction on Pt(100), Rus. J. Electrochem. 48 (2012) 302–315.
[22] E.B. Molodkina, I.G. Botryakova, A.I. Danilova, J. Souza-Garcia, J.M. Feliu, Kinetics and mechanism of nitrate and nitrite electroreduction on Pt(100) electrodes modified by copper adatoms, Rus. J. Electrochem. 49 (2013) 285–293.
[23] S.E. Bae, K.L. Stewart, A.A. Gewirth, Nitrate adsorption and reduction on Cu(100) in acidic solution, J. Am. Chem. Soc. 129 (2007) 10171–10180.
[24] S.E. Bae, A.A. Gewirth, Differential reactivity of Cu(111) and Cu(100) during nitrate reduction in acid electrolyte, Faraday Discuss. 140 (2008) 113–123.
[25] T. Chen, H. Li, H. Ma, M.T.M. Koper, Surface modification of Pt(100) for electrocatalytic nitrate reduction to dinitrogen in alkaline solution, Langmuir 31 (2015) 3277–3281.
[26] S. Garbarino, A. Ponrouch, S. Pronovost, J. Gaudet, D. Guay, Synthesis and characterization of preferentially oriented (100) Pt nanowires, Electrochem. Commun. 11 (2009) 1924–1927.
[27] A. Ponrouch, S. Garbarino, E. Bertin, C. Andrei, G.A. Botton, D. Guay, Highly porous and preferentially oriented {100} platinum nanowires and thin films, Adv. Funct. Mater. 22 (2012) 4172–4181.
[28] E. Bertin, C. Roy, S. Garbarino, D. Guay, J. Solla-Gullón, F.J. Vidal-Iglesias, J.M. Feliu, Effect of the nature of (100) surface sites on the electroactivity of macroscopic Pt electrodes for the electrooxidation of ammonia, Electrochem. commun. 22 (2012) 197–199.
[29] E. Bertin, S. Garbarino, D. Guay, J. Solla-Gullón, F.J. Vidal-Iglesias, J.M. Feliu, Electrodeposited platinum thin films with preferential (100) orientation: characterization and electrocatalytic properties for ammonia and formic acid oxidation, J. Power Sources 225 (2013) 323–329.
[30] C. Roy, E. Bertin, M.H. Martin, S. Garbarino, D. Guay, Hydrazine oxidation at porous and preferentially oriented {100} Pt thin films, Electrocatalysis 4 (2013) 76–84.
[31] E. Bertin, S. Garbarino, D. Guay, Formic acid oxidation on Bi covered Pt electrodeposited thin films: influence of the underlying structure, Electrochim. Acta 134 (2014) 486–495.

[32] E. Bertin, A. Fleury, C. Roy, M.H. Martin, S. Garbarino, D. Guay, Preferentially (100) oriented Pt thin Film with less than a monolayer of Bi, Pd and Sb adatoms: application for formic acid oxidation, Electrochim. Acta 162 (2015) 237–244.
[33] E. Bertin, S. Garbarino, D. Guay, Formic acid oxidation on antimony-covered platinum films with a preferential (100) orientation, J. Power Sources 299 (2015) 315–323.
[34] C. Fisica, U. Milano, Real surface area measurements in electrochemistry, Int. Union Pure Appl. Chem. 63 (1991) 711–734.
[35] J. Solla-Gullon, F.J. Vidal-Iglesias, P. Rodrıguez, E. Herrero, J.M. Feliu, J. Clavilier, A. Aldaz, In situ surface characterization of preferentially oriented platinum nanoparticles by using electrochemical structure sensitive adsorption reactions, J. Phys. Chem. B 108 (2004) 13573–13575.
[36] D.J. Jenkins, A.M.S. Alabdulrahman, G.A. Attard, K.G. Griffin, P. Johnston, P.B. Wells, Enantioselectivity and catalyst morphology: step and terrace site contributions to rate and enantiomeric excess in Pt-catalysed ethyl pyruvate hydrogenation, J. Catal. 234 (2005) 230–239.
[37] J. Solla-Gullón, P. Rodríguez, E. Herrero, A. Aldaz, J.M. Feliu, Surface characterization of platinum electrodes, Phys. Chem. Chem. Phys. 10 (2008) 1359–1373.
[38] T. Abe, G.M. Swain, K. Sashikata, K. Itaya, Effect of underpotential deposition (UPD) of copper on oxygen reduction at Pt(111) surfaces, J. Electroanal. Chem. 382 (1995) 73–83.
[39] L.J. Buller, E. Herrero, R. Gomez, J.M. Feliu, H.D. Abruña, Induced adsorption of sulfate/bisulfate anions by submonolayeramounts of copper on deliberately stepped Pt surfaces, J. Chem. Soc. Faraday Trans. 92 (1996) 3757–3762.
[40] C. Nishihara, H. Nozoye, Underpotential deposition of copper on Pt(S)-[n(111) × (100)] electrodes in sulfuric acid solution, J. Electroanal. Chem. 386 (1995) 75–82.
[41] R. Francke, V. Climent, H. Baltruschat, J.M. Feliu, Electrochemical deposition of copper on stepped platinum surfaces in the [0 1 1] zone vicinal to the (1 0 0) plane, J. Electroanal. Chem. 624 (2008) 228–240.
[42] M. Pourbaix, Atlas of Electrochemical Equilibria in Aqueous Solutions, Houston Texas: National Association of Corrosion Engineers, 1974. Print.
[43] C. Nishihara, H. Nozoye, Underpotential deposition of copper on Pt(S)-[n(111) × (100)] electrodes in sulfuric acid solution, J. Electroanal. Chem. 386 (1995) 75–82.
[44] C.L. Green, A. Kucernak, Determination of the platinum and ruthenium surface areas in platinum-Ruthenium alloy electrocatalysts by underpotential deposition of copper. I. unsupported catalysts, J. Phys. Chem. B 106 (2002) 1036–1047.
[45] H. Herrero, L.J. Buller, H.D. Abruna, Underpotential deposition at single crystal surfaces of Au, Pt, Ag and Other Materials, Chem. Rev. 101 (2001) 1897–1930.
[46] A.S. Varela, C. Schlaup, Z.P. Jovanov, P. Malacrida, S. Horch, I.E.L. Stephens, I. Chorkendorff, $CO_2$ electroreduction on well-defined bimetallic surfaces: Cu overlayers on pt(111) and Pt(211), J. Phys. Chem. C 117 (2013) 20500–20508.
[47] R. Reske, M. Duca, M. Oezaslan, K.J.P. Schouten, M.T.M. Koper, P. Strasser, Controlling catalytic selectivities during $CO_2$ electroreduction on thin Cu metal overlayers, J. Phys. Chem. Lett. 4 (2013) 2410–2413.
[48] S.M. Alia, B.S. Pivovar, Y. Yan, Platinum-Coated copper nanowires with high activity for hydrogen oxidation reaction in base, J. Am. Chem. Soc. 135 (2013) 13473–13478.
[49] A.J. Bard, L.R. Faulkner, Electrochemical methods: fundamentals and applications, 2nd ed., Wiley, 2001.
[50] M. Duca, M.C. Figueiredo, V. Climent, P. Rodriguez, J.M. Feliu, M.T.M. Koper, Selective catalytic reduction at quasi-Perfect Pt(100) domains: a universal low-temperature pathway from nitrite to $N_2$, J. Am. Chem. Soc. 133 (2011) 10928–10939.